Synthesis and Properties of ABA and ABC Triblock Copolymers with Glassy (A), Elastomeric (B), and Crystalline (C) Blocks

Holger Schmalz,[†] Alexander Böker,[†,‡] Ronald Lange,[§] Georg Krausch,[‡] and Volker Abetz*[,†]

Makromolekulare Chemie II, Universität Bayreuth, 95440 Bayreuth, Germany; Physikalische Chemie II and Bayreuther Zentrum für Kolloide und Grenzflächen (BZKG), Universität Bayreuth, 95440 Bayreuth, Germany; and DSM Research, 6160 MD Geleen, The Netherlands

Received May 22, 2001

ABSTRACT: We describe the synthesis, characterization, and properties of polystyrene-*block*-poly(ethylene-*alt*-propylene)-*block*-polyethylene (PS-*b*-PEP-*b*-PE) and polystyrene-*block*-poly(ethylene-*alt*-propylene)-*block*-polystyrene (PS-*b*-PEP-*b*-PS) triblock copolymers. Morphological investigations using TEM, SEM, and SFM reveal for the PS-*b*-PEP-*b*-PE triblock copolymers a morphology consisting of PS cylinders and PE crystallites within a matrix of the PEP block, whereas the PS-*b*-PEP-*b*-PS triblock copolymer shows interconnected, distorted PS cylinders in the PEP matrix. Mechanical characterization of these triblock copolymers demonstrated that for small strains the PS-*b*-PEP-*b*-PE triblock copolymers exhibit the aimed smaller plastic deformations, i.e. better elastic properties, compared to the polystyrene-based ABA type thermoplastic elastomer. However, at high strains the PS-*b*-PEP-*b*-PS triblock copolymer shows a significantly better elastic recovery. The high plastic set at high elongations in PS-*b*-PEP-*b*-PE triblock copolymers is attributed to the weaker resistance of the PE crystallites compared to amorphous PS domains in the PS-*b*-PEP-*b*-PS triblock copolymer.

Introduction

Linear ABA triblock copolymers, with the A-block consisting of polystyrene and the B-block typically polybutadiene or polyisoprene (PS-*b*-PB-*b*-PS or PS-*b*-PI-*b*-PS), are classic thermoplastic elastomers.[1−3] Because of the incompatibility between the two components, microphase separation occurs whereby the polystyrene minority phase forms dispersed spheres or cylinders in a rubbery matrix of the middle block. Linear ABC triblock copolymers have been investigated by several groups and a huge variety of morphologies was found.[4−7] Besides classes of lamellar,[8,9] cylindrical,[10,11] and spherical morphologies,[12] also cocontinuous morphologies were found,[13−15] which all relate to the corresponding morphologies known from binary block copolymers. Fundamentally different from the diblock copolymer morphologies is the "knitting pattern" found for particular polystyrene-*block*-poly(ethylene-*stat*-butylene)-*block*-poly(methyl methacrylate) triblock copolymers.[16−18] A problem encountered in ABC triblock copolymers with short end blocks (i.e., end blocks forming spheres or cylinders) is the common occurrence of at least partial miscibility between the two end blocks. In such cases a two-phase morphology is obtained rather than a three-phase morphology. As a consequence, the B chain may loop back into the same end block domain rather than being forced to form a bridge between two different end block domains. This should have an influence on the elastic properties of such a material, since bridges and loops should behave differently. In conclusion, ABC triblock copolymers with mixed end blocks should behave like ABA triblock copolymers in terms of both their morphological and mechanical properties.

ABC triblock copolymers offer the ability to build thermoplastic elastomers without any loops, if the A- and C-blocks are immiscible. Since the immiscibility is a function of the product $\chi_{AC}N_{AC}$, either strongly incompatible components or a high degree of polymerization has to be used (N_{AC} is the degree of polymerization of the A- and C-block, and χ_{AC} is the segmental interaction parameter between the two species).[19] A high degree of polymerization, however, results in a high melt viscosity, which is disadvantageous in view of processing demands. For polystyrene-*block*-polybutadiene-*block*-poly(methyl methacrylate) (PS-*b*-PB-*b*-PMMA) triblock copolymers, it was shown that only systems with a rather high molecular weight display microphase-separated PS and PMMA domains under favorable conditions.[20,21]

Semicrystalline end blocks offer a way to achieve segregated end blocks at low molecular weights, since crystallization is a strong driving force for microphase separation. Investigations on polyethylene-*block*-poly(ethylene-*alt*-propylene) (PE-*b*-PEP) diblock copolymers show that even for low molecular weights a microphase-separated structure is obtained due to crystallization-induced microphase separation.[22−24] Furthermore, this system exhibits a small value for the segmental interaction parameter χ of 0.007 at 120 °C (above the melting point of PE), resulting in a homogeneous melt in a wide composition range which is advantageous in view of processing.[25]

ABA triblock copolymers with polyethylene as crystallizable A-block have already been investigated with respect to their morphology and mechanical properties.[26−33] Morton and co-workers compared polyethylene-*block*-polyisoprene-*block*-polyethylene (PE-*b*-PI-*b*-PE) and polyethylene-*block*-poly(ethylene-*stat*-butylene)-

[†] Makromolekulare Chemie II, Universität Bayreuth.
[‡] Physikalische Chemie II and BZKG, Universität Bayreuth.
[§] DSM Research.
* Corresponding author. e-mail: volker.abetz@uni-bayreuth.de.

10.1021/ma010875d CCC: $20.00
Published on Web 11/02/2001

block-polyethylene (PE-*b*-PEB-*b*-PE) triblock copolymers with polystyrene-based thermoplastic elastomers. The polyethylene-containing thermoplastic elastomers exhibit better solvent resistance and show a homogeneous melt in the case of the PE-*b*-PEB-*b*-PE systems. Triblock copolymers with polyethylene contents up to 30 wt % show an elastomeric behavior with low plastic deformations after elongation, whereas systems with higher polyethylene content exhibit more plastic properties. Compared to the polystyrene-based thermoplastic elastomers, the plastic deformations even for the systems with 30 wt % polyethylene are higher especially for high extensions. This may be attributed to a weaker resistance of crystalline domains to distortion compared to polystyrene domains in this case. The Young's modulus increases with increasing polyethylene content, whereby the tensile strength mainly depends on the molecular weight of the polyethylene block.

In this contribution we compare ABC triblock copolymers with a glassy and a semicrystalline end block with an ABA triblock copolymer with glassy end blocks. Here we describe the synthesis and the properties of polystyrene-*block*-poly(ethylene-*alt*-propylene)-*block*-polyethylene (PS-*b*-PEP-*b*-PE) triblock copolymers. Tensile testing in comparison to polystyrene-*block*-poly(ethylene-*alt*-propylene)-*block*-polystyrene (PS-*b*-PEP-*b*-PS) triblock copolymers is performed in order to investigate the influence of a crystalline end block on the mechanical properties. A special synthetic procedure allows us to synthesize PS-*b*-PEP-*b*-PS and PS-*b*-PEP-*b*-PE triblock copolymers with identical A- and B-blocks, only differing in the type of the C-block. This excludes any effects on the mechanical properties resulting from the molecular weight or composition of the triblock copolymers. The miscibility of polyethylene and poly(ethylene-*alt*-propylene) in the melt provides us with systems exhibiting a two-phase melt instead of a three-phase melt. This should in turn result in a reduced melt viscosity and hence in a better processability. Furthermore, the low solubility of the polyethylene block compared to a polystyrene block should also lead to a higher solvent resistance of the corresponding triblock copolymers.

It should be noted that in general ABA and ABC triblock copolymers with a similar overall composition with respect to the end blocks must have different morphologies, when A and C are immiscible. For example, when A and C form cylinders, they must be arranged on a tetragonal lattice or a hexagonal lattice having a different symmetry compared to the hexagonally packed cylinders of the corresponding ABA triblock copolymer. The situation is similar in a lattice of A and C spheres in a B matrix. Thus, an investigation of mechanical properties in dependence on the presence or absence of loops without changing the morphology is impossible when comparing ABA and ABC triblock copolymers. It is the aim of this contribution to show a way to generate ABC triblock copolymers with short microphase-separated end blocks and compare them with a reference ABA triblock copolymer.

Experimental Section

Materials. Benzene (Acros) was purified by successive distillation over CaH_2 and potassium and kept in a dry nitrogen atmosphere until use. Styrene (Acros) was distilled from CaH_2 under nitrogen, stirred over Bu_2Mg, and condensed into storage ampules. Butadiene (Linde) was passed over columns with molecular sieve and activated alumina, followed by storage over Bu_2Mg under purified nitrogen before use. Isoprene (Fluka) was stirred over Bu_2Mg under purified nitrogen for 12 h and condensed onto *n*-BuLi followed by stirring at 0 °C for 1 h before being condensed into glass ampules. Toluene (p. a., Merck), *sec*-BuLi (Acros, 1.3 M in cyclohexane/hexane: 92/8), *n*-BuLi (Aldrich, 1.6 M in hexane), Bu_2Mg (Aldrich, 1 M in heptane), and Wilkinson catalyst $(Ph_3P)_3Rh(I)Cl$ (Aldrich) were used as received.

Synthesis. The synthesis of PS-*b*-PI-*b*-PB and PS-*b*-PI-*b*-PS triblock copolymers was accomplished by sequential anionic polymerization of styrene, isoprene, and butadiene or styrene in benzene at 40 °C (for styrene) and 60 °C (for butadiene and isoprene) with *sec*-BuLi as initiator. The use of benzene as a solvent results in a high 1,4-addition for butadiene and isoprene which particularly for butadiene is indispensable to get a "pseudo-polyethylene" structure after hydrogenation. The combination of two laboratory autoclaves (Büchi) allowed us to synthesize ABC triblock copolymers with identical A- and B-blocks but different C-blocks by dividing the living AB diblock copolymer precursor into two fractions. This enables us to study the influence of the C end block on the morphological and mechanical properties of ABC triblock copolymers by keeping all other parameters, like molecular weight and relative composition, constant.

Hydrogenation. The PS-*b*-PEP-*b*-PE and PS-*b*-PEP-*b*-PS triblock copolymers were synthesized by hydrogenation of the corresponding precursor polystyrene-*block*-poly(1,4-isoprene)-*block*-poly(1,4-butadiene) (PS-*b*-PI-*b*-PB) and polystyrene-*block*-poly(1,4-isoprene)-*block*-polystyrene (PS-*b*-PI-*b*-PS). Homogeneous catalytic hydrogenation was carried out in degassed toluene (1.5−2 wt % solution of polymer) at 100 °C and 90 bar H_2 pressure for 3 days using Wilkinson catalyst (1 mol % with respect to the number of double bonds). Purification was accomplished by precipitation in methanol. The extent of hydrogenation was verified using ^1H NMR spectroscopy (Bruker AC 250 spectrometer). Under the used conditions the polybutadiene blocks are hydrogenated completely, and the polyisoprene blocks show an almost complete saturation with ≤1% residual double bonds.

Size Exclusion Chromatography (SEC). SEC experiments were performed on a Waters instrument calibrated with narrowly distributed polystyrene standards at 30 °C. Four PSS-SDV columns (5 μ, Polymer Standards Service, Mainz) with a porosity range from 10^2 to 10^5 Å were used together with a differential refractometer and a UV detector at 254 nm. Measurements on the non-hydrogenated triblock copolymers were performed in THF with a flow rate of 1 mL/min using toluene as internal standard.

Differential Scanning Calorimetry (DSC). For thermal analysis a Perkin-Elmer DSC 7 with a CCA 7 liquid nitrogen cooling device was used. For all measurements a two-point calibration with chloroform and indium was applied. All experiments were performed at a heating rate of 10 K/min, unless otherwise specified. The displayed heating trace corresponds to the second heating run in order to exclude effects resulting from any previous thermal history of the samples.

Dynamic Mechanical Analysis. Dynamic shear experiments were performed with an Advanced Rheometric Expansion System (ARES, Rheometrics) in the plate−plate configuration with a plate diameter of 25 mm and a gap of ≈1 mm. Temperature-dependent measurements of G' and G'' were performed at a scanning rate of 1 K/min at a constant frequency of 1 rad/s. It was made sure that all experiments were done in the linear viscoelastic regime.

Mechanical Testing. Mechanical testing was carried out using an Instron 5565 and a Zwick (equipped with optical extensometers) tensile testing machine. Young's modulus was determined at a testing speed of 0.2 mm/min at small elongations (0−0.5%); elongations at break were measured at 20 mm/min. Hysteresis measurements were performed at a testing speed of 20 mm/min for elongations to 100 (3 times), 200, 300, 400, and 500% followed by extension to break. No holding time between the cycles was applied. Test specimens according to ISO 37:1994 were used. Preparation was accomplished by compression molding into plates at 140−150 °C followed by

cooling to room temperature (≈−1.5 K/min). It was made sure that the cutting of test specimens always occurred in the same direction in order to exclude any effects resulting from different orientation within the test samples.

Transmission Electron Microscopy (TEM). The bulk morphology of the triblock copolymers was examined by bright field TEM using a Zeiss CEM 902 electron microscope operated at 80 kV. Films of PS-*b*-PI-*b*-PS triblock copolymers (around 0.5 mm thick) were prepared by casting from a 2 wt % solution in $CHCl_3$ and allowed to slowly evaporate over a period of 2 weeks followed by drying under vacuum for 1 day. In addition, compression-molded samples, which were used for mechanical testing, were also taken for morphological investigations. Thin sections were cut at −130 °C using a Reichert-Jung Ultracut E microtome equipped with a diamond knife. Selective staining of the PI domains was achieved by exposure of the sections to OsO_4 vapor for 60 s, while the thin sections of hydrogenated triblock copolymers were exposed to RuO_4 vapor for 45 min to selectively stain the PS domains.

Scanning Electron Microscopy (SEM). SEM images were taken on a LEO 1530 Gemini instrument equipped with a field emission cathode possessing a lateral resolution of approximately 2 nm. Thin films of PS-*b*-PEP-*b*-PE were prepared by dip coating onto a polished silicon wafer from a 1 mg/mL solution of the triblock copolymer in toluene. The films were stained with RuO_4 vapor for 45 min prior to SEM imaging in order to visualize the PS domains.

Scanning Force Microscopy (SFM). Scanning force microscopy images were taken on a Digital Instruments Dimension 3100 microscope operated in TappingMode (free amplitude of the cantilever: 20 nm; set point ratio: 0.95). Measurements were performed on thin films prepared on polished silicon wafers by dip coating from a 1 mg/mL solution of the polymer in toluene or by spin-coating using a 5 wt % solution of the respective polymer in toluene. Selective swelling of the PS-microdomains in PS-*b*-PEP-*b*-PE triblock copolymer thin films was accomplished by exposing a vacuum-dried film to toluene vapor for 1 min. In addition, measurements were performed on compression-molded samples, which were prepared similar to the samples used for mechanical testing. SFM imaging was carried out on smooth cut surfaces obtained by cutting with a diamond knife at −130 °C using a Reichert-Jung Ultracut E microtome.

Small-Angle X-ray Scattering (SAXS). SAXS measurements were performed on compression-molded samples using a Bruker-AXS Nanostar instrument with a sealed X-ray tube (Cu, $\lambda = 1.5418$ Å) operated at 40 mA and 40 kV and equipped with crossed Goebel mirrors and a 2D Histar detector.

Results and Discussion

Synthesis. The PS-*b*-PEP-*b*-PE and PS-*b*-PEP-*b*-PS triblock copolymers were prepared by homogeneous catalytic hydrogenation of the corresponding PS-*b*-PI-*b*-PB and PS-*b*-PI-*b*-PS triblock copolymers which were synthesized by sequential anionic synthesis.

Scheme 1 shows the synthesis of PS-*b*-PI-*b*-PB and PS-*b*-PI-*b*-PS triblock copolymers with identical PS- and PI-blocks by combination of two laboratory autoclaves. First the sequential anionic polymerization of styrene and isoprene was performed in benzene. Subsequently, the resulting solution of living PS-*b*-PI diblock copolymer precursors was divided into two fractions. Further addition of styrene or butadiene respectively leads to the formation of the corresponding PS-*b*-PI-*b*-PS and PS-*b*-PI-*b*-PB triblock copolymers. Polymerization in benzene results in a high 1,4-content for butadiene and isoprene as depicted in Table 1. In our nomenclature ($A_xB_yC_z{}^m$) the subscripts give the weight percentage of the corresponding block, and the superscript is the molar mass of the triblock copolymer in kg/mol. SEC shows that dividing the living PS-*b*-PI diblock copolymer precursor proceeds without any termination, resulting in narrowly distributed PS-*b*-PI-*b*-P(S/B) triblock copolymers (Figure 1, Table 1). However, for the PS-*b*-PI-*b*-PB triblock copolymers the addition of butadiene to the living PS-*b*-PI precursor gives rise to a very small amount of chain termination (<6%) as can be seen from the shoulder at higher elution volumes (Figure 1) which might be attributed to residual impurities in the butadiene. Because of the very small extent of chain termination, the residual PS-*b*-PI precursor is not expected to influence the mechanical properties of the PS-*b*-PI-*b*-PB triblock copolymer after hydrogenation.

Homogeneous catalytic hydrogenation was carried out in toluene using the Wilkinson catalyst $(Ph_3P)_3Rh(I)Cl$ at 100 °C and 90 bar H_2 pressure. Under these conditions, the PB-block gets completely hydrogenated and the PI-block exhibits an almost complete saturation with less than 1% residual double bonds, as monitored by the disappearance of the corresponding signals of the vinylic protons in ^1H NMR (not shown). Hydrogenation at lower temperatures (60 °C) leads only to a partially

Scheme 1. Synthesis of Polystyrene-*block*-poly(1,4-isoprene)-*block*-polystyrene (PS-*b*-PI-*b*-PS) and Polystyrene-*block*-poly(1,4-isoprene)-*block*-poly(1,4-butadiene) (PS-*b*-PI-*b*-PB) with Identical PS- and PI-Blocks by Combination of Two Laboratory Autoclaves

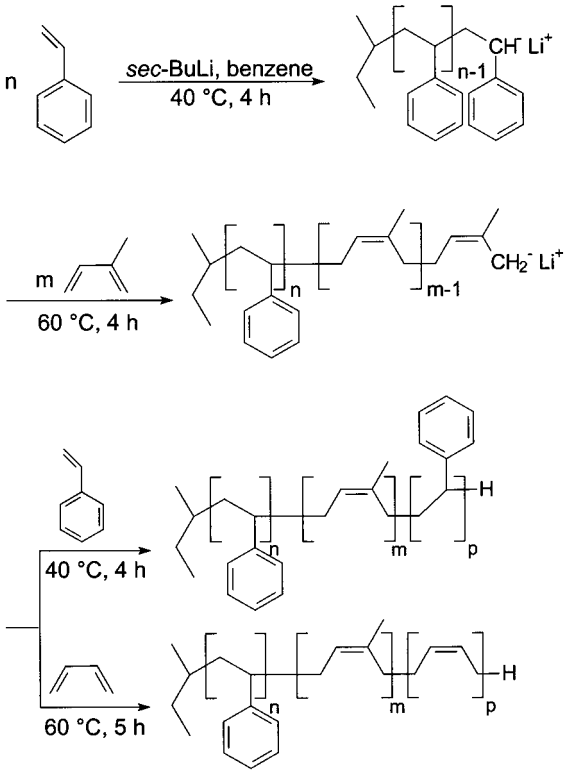

Table 1. Molecular Weight Characterization and Microstructure of PS-*b*-PI-*b*-P(B/S) Triblock Copolymers

triblock	$M_n{}^a$ [kg/mol]	$M_w/M_n{}^b$	PB-block[c] % 1,4	PB-block[c] % 1,2	PI-block[c] % 1,4	PI-block[c] % 1,2	PI-block[c] % 3,4
$S_{14}I_{57}B_{29}{}^{109}$	109	1.02	89	11	92	4	4
$S_{14}I_{64}B_{22}{}^{119}$	119	1.02	87	13	92	4	4
$S_{14}I_{65}S_{21}{}^{117}$	117	1.01			92	4	4

[a] Determined by ^1H NMR spectroscopy using the molecular weight of the PS precursor obtained by SEC in THF calibrated against PS standards. [b] Determined by SEC in THF calibrated against PS standards. [c] Determined by ^1H NMR spectroscopy in $CDCl_3$.

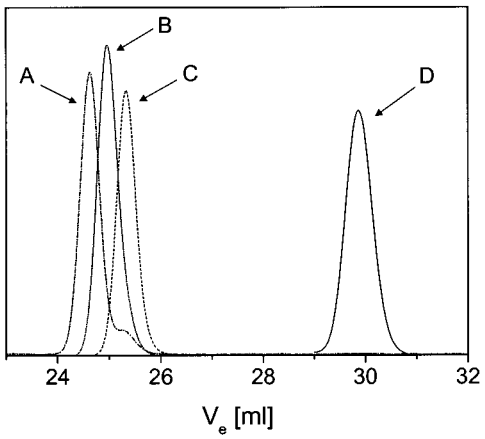

Figure 1. SEC traces of a PS-*b*-PI-*b*-PS (B) and a PS-*b*-PI-*b*-PB (A) triblock copolymer with identical PS and PI blocks, synthesized by connection of two laboratory autoclaves, including the PS (D) and PS-*b*-PI (C) precursors using THF as eluent and toluene as internal standard.

Table 2. DSC Data of PS-*b*-PEP-*b*-P(E/S) Triblock Copolymers[a]

triblock	$T_{G,PEP}$ [°C]	$T_{G,PS}$ [°C]	$T_{m,PE}$ [°C]	$T_{c,PE}$ [°C]	α_{PE} [%]
$S_{14}EP_{66}S_{20}^{119}$	−55.5	102.4			
$S_{14}EP_{64}E_{22}^{122}$	−56.0	99.3[b]	88.0	57.6	31.9
$S_{13}EP_{57}E_{30}^{112}$	−56.0	100.4[b]	88.7	59.8	31.0

[a] T_m = melting point (peak maximum), T_c = crystallization temperature (peak maximum), α = degree of crystallinity, and T_G = glass transition temperature. [b] Determined by dynamic mechanical analysis (maximum G'', 1 rad/s, 1 K/min).

hydrogenated PI-block, whereas the PB-block gets completely saturated.

Thermal Properties. The PS-*b*-PEP-*b*-PS and PS-*b*-PEP-*b*-PE triblock copolymers exhibit glass transition temperatures at approximately −55 °C for the PEP block and at about 100 °C for the PS block, reflecting a strongly microphase-separated structure (Table 2). The PE blocks in PS-*b*-PEP-*b*-PE triblock copolymers reveal a melting endotherm at ca. 90 °C and degrees of crystallinity of $\alpha \approx 31\%$. The degree of crystallinity was calculated using the heat of fusion for a 100% crystalline PE of $\Delta H_m^0 = 276.98$ J/g.[34] The DSC heating trace for $S_{13}EP_{57}E_{30}^{112}$ (Figure 2) displays a relatively broad melting endotherm for the PE block, indicating a broad crystallite size distribution. The latter may arise from the approximately 11% 1,2-units in the corresponding PB block of the non-hydrogenated triblock copolymer precursor (Table 1). The corresponding cooling trace (Figure 2) shows that crystallization of the PE block occurs at ca. 60 °C. The melting and crystallization temperatures of the PE block in the PS-*b*-PEP-*b*-PE triblock copolymers exhibit a slight increase with increasing molecular weight of the PE block (Table 2). In addition, the degree of crystallinity α(PE) shows a slight increase with increasing molecular weight of the triblock copolymer, which might be attributed to a higher incompatibility between the PEP and PE block due to the increasing values of χN. From DSC measurements it is not possible to detect a glass transition temperature of the PS block in PS-*b*-PEP-*b*-PE triblock copolymers. In Figure 3 a temperature-dependent dynamic shear experiment on $S_{13}EP_{57}E_{30}^{112}$ is shown. The sharp drop in the storage modulus G' at ca. −50 °C is related to the glass transition temperature of the PEP block which corresponds to the transition temperature obtained by

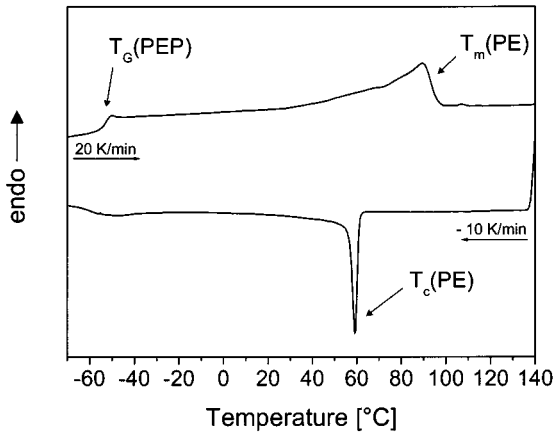

Figure 2. DSC heating and cooling traces for $S_{13}EP_{57}E_{30}^{112}$.

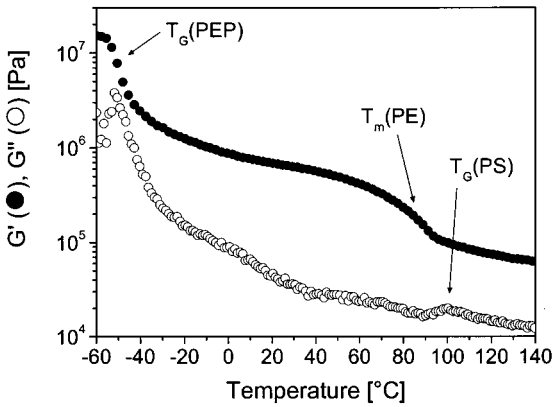

Figure 3. Temperature-dependent dynamic shear experiments on $S_{13}EP_{57}E_{30}^{112}$.

DSC (Table 2, Figure 2). Upon further heating, melting of the crystalline PE block results in an additional drop in G' at ca. 90 °C, which is in line with the observed melting endotherm in DSC. The glass transition temperature of the PS block is indicated by a small maximum in the loss modulus G'' at ca. 100 °C. The corresponding drop in G' is not visible, probably due to the low PS content of only 13 wt %.

Concerning the solubility, PS-*b*-PEP-*b*-PE triblock copolymers show a better solvent resistance compared to PS-*b*-PEP-*b*-PS triblock copolymers, which are in general soluble in organic solvents. In $CHCl_3$ and toluene small amounts of PS-*b*-PEP-*b*-PE triblock copolymers are soluble at room temperature, whereas higher concentrated solutions (>0.02 g/mL) can only be obtained at elevated temperatures and exhibit gelation upon cooling.

Morphology. TEM investigations on $S_{14}I_{65}S_{21}^{117}$ (precursor of $S_{14}EP_{66}S_{20}^{119}$) cast from $CHCl_3$ solution show a cylindrical morphology with hexagonally packed PS-cylinders within a matrix of PI (selectively stained with OsO_4 vapor) as shown in Figure 4A. With regard to the performed mechanical testing, the morphology of the compression-molded samples is of special interest. Figure 4B shows a TEM image of $S_{14}I_{65}S_{21}^{117}$, prepared by compression-molding in an identical way as for the tensile testing. The PS-domains exhibit a strongly distorted cylindrical structure without showing any long-range order. The TEM image of the corresponding hydrogenated triblock copolymer $S_{14}EP_{66}S_{20}^{119}$ (Figure 4C), also prepared by compression-molding, exhibits a similar morphology consisting of strongly distorted PS-

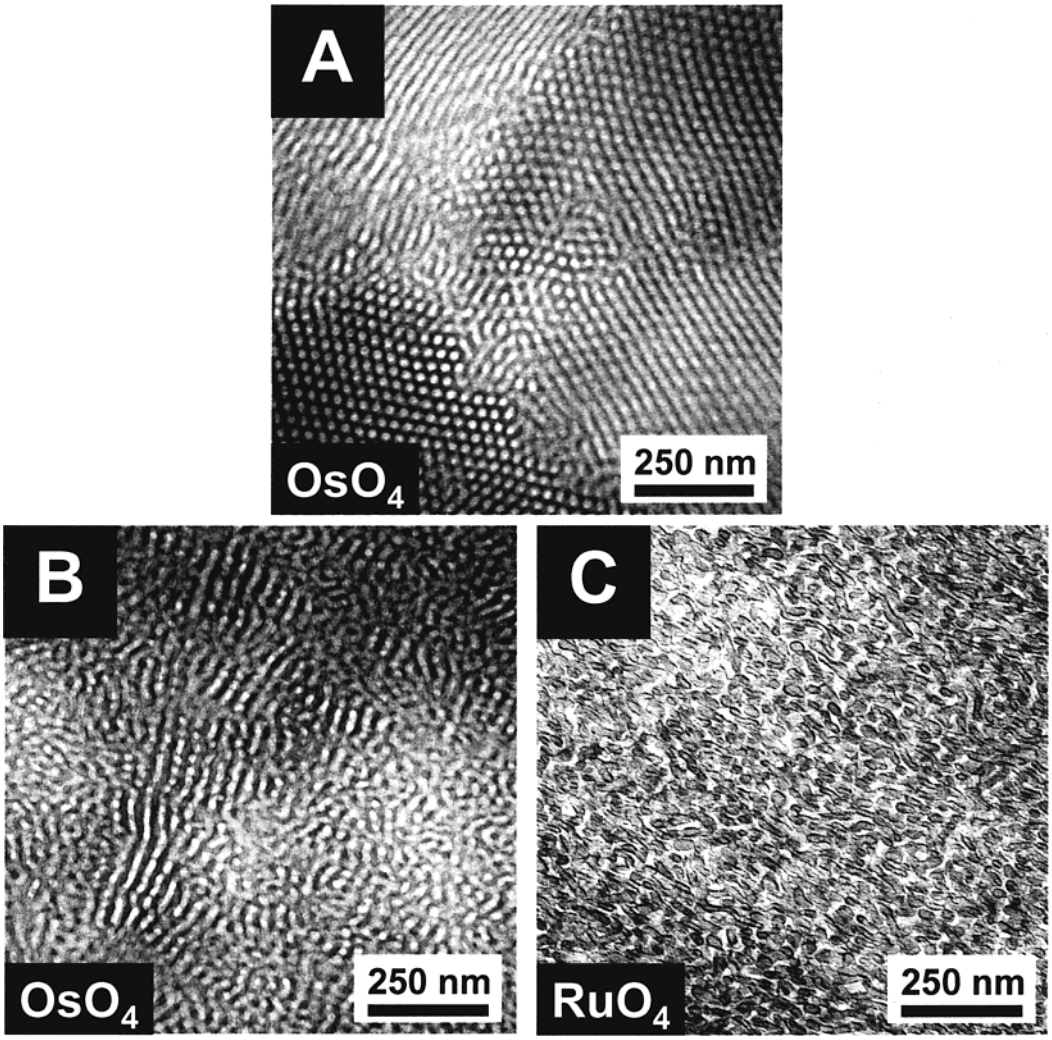

Figure 4. TEM images of (A) $S_{14}I_{65}S_{21}^{117}$ cast from $CHCl_3$, (B) $S_{14}I_{65}S_{21}^{117}$ prepared by compression-molding, selective staining of PI was achieved by exposure to OsO_4 vapor, and (C) $S_{14}EP_{66}S_{20}^{119}$ prepared by compression-molding, stained with RuO_4 for visualization of PS.

cylinders. In both systems the formation of interconnected PS-cylinders is possible due to the strongly distorted PS-domains.

Morphological investigations on PS-*b*-PEP-*b*-PE triblock copolymers using conventional TEM techniques encounter the problem that the PS and PE domains cannot be visualized simultaneously.[35] Detection of the PS-domains is possible by selective staining of PS with RuO_4 vapor. The PE crystallites can be visualized by underfocus phase contrast bright field TEM investigations of the unstained samples. To gain a more detailed insight into the morphology of our PS-*b*-PEP-*b*-PE triblock copolymers, we prepared thin films by dip and spin-coating from dilute solutions. Figure 5A shows the SEM image of such a thin film of $S_{13}EP_{57}E_{30}^{112}$ prepared from toluene solution (1 mg/mL). The white dot- and wormlike structures represent the PS domains selectively stained by exposure to RuO_4 vapor. As the PE block is expected to form crystalline lamellae, it is very likely that according to the composition the PS block forms cylinders in the PEP matrix. The cause of the obvious distortion of the PS cylinders will be explained in the following.

Figure 5B shows a SFM phase contrast image of a vacuum-dried thin film of $S_{13}EP_{57}E_{30}^{112}$ dip-coated from toluene solution (1 mg/mL). In this picture we can distinguish between at least two different phases. The bright elongated domains with rough boundaries correspond to PE crystallites which induce a high phase shift within a matrix of PEP which appears darker in the phase contrast. In addition, we can identify a third phase which is located in between the PE crystallites. This phase can be visualized more clearly by exposure of the film to toluene vapor for 1 min as shown in Figure 5C (circles in Figure 5B,C). As toluene is a selective solvent for polystyrene, we can conclude that the bright dot- and wormlike structures can be attributed to PS cylinders in a PEP matrix located between PE crystallites. Obviously, the swelling of the PS domains with toluene also changes the interaction between the tip and the sample surface significantly, which leads to a distinct phase shift. As during film preparation, the PE crystallizes before solidification of the PS cylinders; the latter have to cope with the confined geometry given by the PE "crystal lamellae", which leads to the observed distortions in the PS-domains.

Further evidence for our phase assignment is given by the SFM images of a spin-coated film of $S_{14}EP_{64}E_{22}^{122}$ (5 wt % solution in toluene, film thickness = 22.6 nm) as shown in Figures 5D,E. The phase image exhibits the same characteristics as the one shown in Figure 5C. In addition, we compare the phase to the respective topography. In both images we can identify the PS-domains (as the lower parts in the topography and the

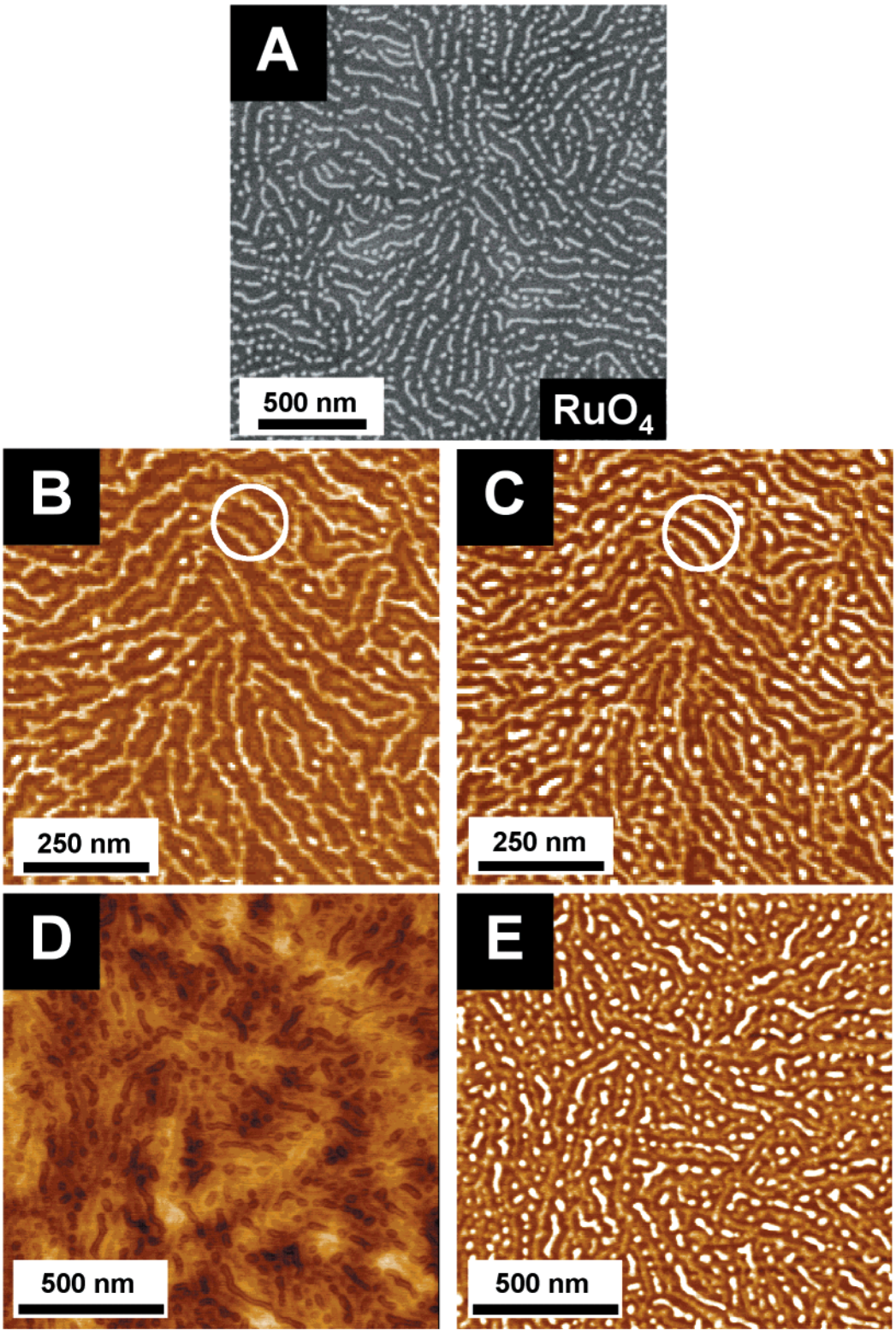

Figure 5. (A) SEM image of a dip-coated film of $S_{13}EP_{57}E_{30}^{112}$ onto a silicon wafer. (B, C) TappingMode SFM phase contrast images of a thin film of $S_{13}EP_{57}E_{30}^{112}$ dip-coated onto a silicon wafer: (B) dry film, (C) same spot of the film after 1 min exposure to toluene vapor, visualizing the PS-cylinders; *z* range = 20°. TappingMode SFM height (D, *z* range = 15 nm) and phase (E, *z* range = 50°) image of a thin film of $S_{14}EP_{64}E_{22}^{122}$ spin-coated from a 5 wt % solution in toluene onto a silicon wafer.

bright areas in the phase). This is in exact agreement with previous investigations[36] where it was shown that the block with the best solubility in the solvent from which the film was prepared showed the highest shrinkage upon film drying. SFM investigations on thin films of $S_{14}EP_{64}E_{22}^{122}$ spin-coated from a 10 wt % solution in toluene (film thickness = 55.6 nm) exhibit an identical morphology (results not shown). From the independence of morphology on film thickness we can conclude that the SiO_x surface of the silicon wafer does not show a significant influence on the morphology of the investigated samples. Therefore, we can deduce that by using TappingMode SFM we are able to identify all three components of our triblock copolymers from topography

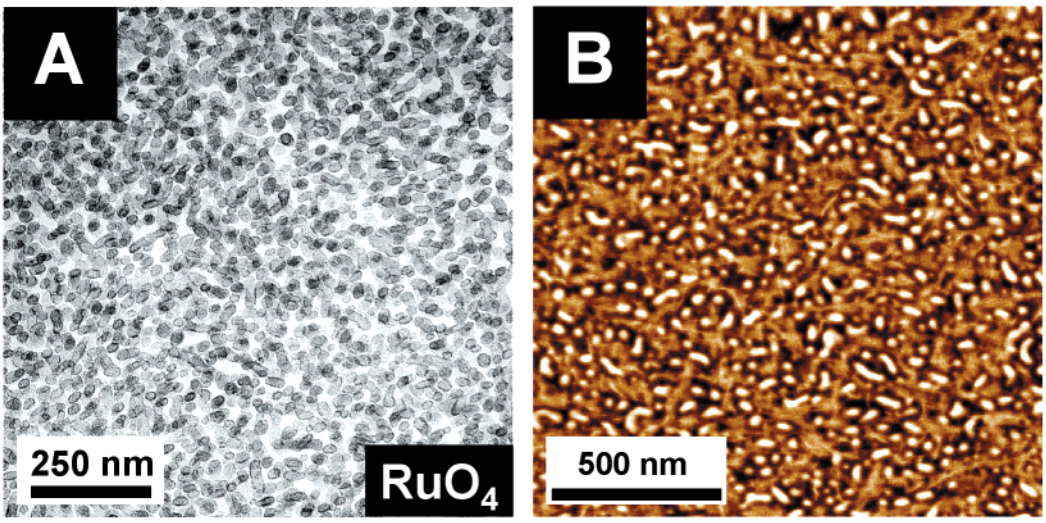

Figure 6. Morphology of $S_{13}EP_{57}E_{30}^{112}$ prepared by compression molding: (A) TEM image; (B) TappingMode SFM phase contrast image (z range = 15°).

Table 3. Mechanical Properties of PS-*b*-PI-*b*-PS and PS-*b*-PEP-*b*-P(E/S) Triblock Copolymers[a]

triblock copolymer	$\epsilon_{plast}(100)/1$ [%]	$\epsilon_{plast}(100)/2$ [%]	$\epsilon_{plast}(100)/3$ [%]	$\epsilon_{plast}(200)$ [%]	$\epsilon_{plast}(300)$ [%]	$\epsilon_{plast}(400)$ [%]	$\epsilon_{plast}(500)$ [%]	E [MPa]	ϵ_{br} [%]
$S_{14}I_{65}S_{21}^{117}$ [b]	11.4 (0.10)	12.0 (0.19)	12.5 (0.52)	19.6 (0.12)	28.3 (0.91)	34.2 (0.26)	40.9 (0.25)	–	1399 (189)
$S_{14}EP_{66}S_{20}^{119}$ [b]	14.2 (0.97)	14.6 (1.26)	14.7 (1.36)	22.4 (0.76)	29.2 (1.04)	42.9 (6.39)	58.1 (4.32)	65.9 (2.00)	844 (14.4)
$S_{14}EP_{64}E_{22}^{122}$ [b]	6.79 (0.89)	7.36 (0.63)	7.75 (0.56)	14.6 (1.11)	26.3 (1.04)	42.5 (0.89)	60.6 (1.83)	9.40 (0.01)	613 (22.8)
$S_{13}EP_{57}E_{30}^{112}$ [b]	7.04 (0.07)	8.06 (0.16)	8.60 (0.10)	17.3 (0.12)	32.7 (0.71)	53.4 (0.92)	76.2 (1.55)	9.83 (0.56)	898 (48.0)
$S_{13}EP_{57}E_{30}^{112}$ [b,c]	7.44 (0.12)	8.16 (0.03)	8.55 (0.10)	16.0 (0.05)	29.6 (0.65)	47.2 (0.32)	67.7 (1.28)	8.53 (0.07)	–
$S_{14}EP_{66}S_{20}^{119}$ [d]	14.1 (1.04)	14.7 (1.08)	15.0 (1.10)	21.5 (1.89)	25.5 (2.74)	27.5 (2.72)	42.6	43.1 (4.21)	–
$S_{14}EP_{64}E_{22}^{122}$ [d]	5.20 (0.39)	5.73 (0.41)	6.03 (0.47)	11.4 (0.86)	20.8 (1.26)	35.5 (1.23)	57.3	10.3 (1.18)	–
$S_{13}EP_{57}E_{30}^{112}$ [d]	5.69 (1.05)	6.36 (1.06)	6.62 (1.08)	13.5 (1.49)	26.2 (1.43)	46.5 (1.19)	72.8	9.70 (0.94)	–

[a] $\epsilon_{plast}(X)$ = remaining plastic deformation after an extension to X%, no holding time in between the steps of the hysteresis measurement; E = Young's modulus; ϵ_{br} = elongation at break; the values in parentheses give the standard deviations. [b] Measurements were performed on an Instron 5565 tensile testing machine without optical extensometers. [c] Sample annealed at 83 °C under vacuum for 12 h. [d] Measurements were performed on a Zwick tensile testing machine equipped with optical extensometers.

and phase information in combination with the influence of selective solvents.

Morphological investigations on PS-*b*-PEP-*b*-PE triblock copolymers were also performed on compression-molded samples, prepared in a similar way as the samples for tensile testing. Figure 6A shows a bright field TEM image of $S_{13}EP_{57}E_{30}^{112}$. Selective staining with RuO_4 vapor visualizes the PS-domains appearing as dark dots and worms, revealing a distorted cylindrical morphology. The PS-domains do not show a preferential orientation as might possibly arise from the compression-molding process. In the SFM phase contrast image, depicted in Figure 6B, clearly three different phases can be distinguished as in the case of the spin-coated sample of $S_{14}EP_{64}E_{22}^{122}$ (Figure 5E). From the results obtained by solvent vapor treatment the bright (higher phase shift) appearing dots and worms can be attributed to PS cylinders in a matrix of the darker appearing PEP block. The third, less bright appearing phase corresponds to crystalline PE domains. Compression-molded samples of $S_{14}EP_{64}E_{22}^{122}$ show an identical overall morphology and differ only in the amount of crystalline PE. Compared to the solvent cast film of $S_{13}EP_{57}E_{30}^{112}$ (Figure 5C) and $S_{14}EP_{64}E_{22}^{122}$ (Figure 5E) the PE crystallites in the compression-molded sample (Figure 6B) are significantly smaller in length and exhibit a more distorted structure. In contrast to the film preparation from solution, the PS solidifies first upon cooling from the melt due to its higher glass transition temperature of ca. 100 °C compared to the crystallization temperature of the PE block of ca. 60 °C (Table 2). Because of the already existing glassy PS domains, the PE blocks have to cope with the confined geometry given by the PS cylinders upon crystallization. This results in the formation of PE crystallites showing smaller dimensions as compared to the PE crystallites formed by crystallization from solution. In conclusion, PS-*b*-PEP-*b*-PE triblock copolymers prepared by compression-molding show a similar morphology compared to the solvent cast films, i.e., dispersed PS cylinders and PE crystallites within a matrix of the PEP block.

From the TEM and SFM investigations on compression-molded samples of PS-*b*-PEP-*b*-PS (Figure 4C) and PS-*b*-PEP-*b*-PE (Figures 6A/B) triblock copolymers, no preferential orientation resulting from the melt processing can be detected, as was also confirmed by SEM and 2D-SAXS (not shown).

Mechanical Properties. To investigate the influence of a crystalline end block on the elastic properties of triblock copolymers, we performed hysteresis measurements on PS-*b*-PEP-*b*-PE triblock copolymers in comparison to a PS-*b*-PEP-*b*-PS triblock copolymer (Table 3). The remaining plastic deformation (ϵ_{plast}) was determined for extensions to 100, 200, 300, 400, and 500%, whereby the first cycle was conducted three times. In Figure 7 the hysteresis measurements performed on $S_{13}EP_{57}E_{30}^{112}$ are shown. As in the case of $S_{14}EP_{64}E_{22}^{122}$, no yield point is observed. This finding might be attributed to dispersed PS- and PE-domains within a matrix of the PEP-block, as revealed by TEM and SFM investigations (Figure 6A,B). The inset to

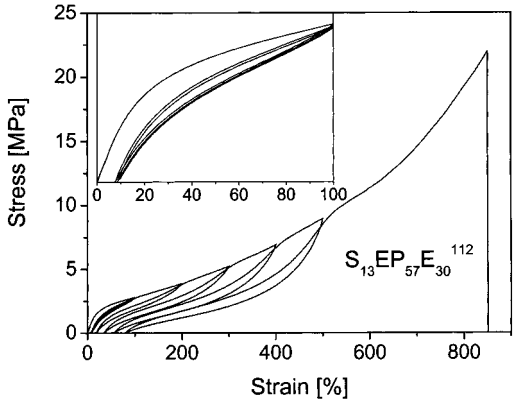

Figure 7. Hysteresis measurements on $S_{13}EP_{57}E_{30}^{112}$.

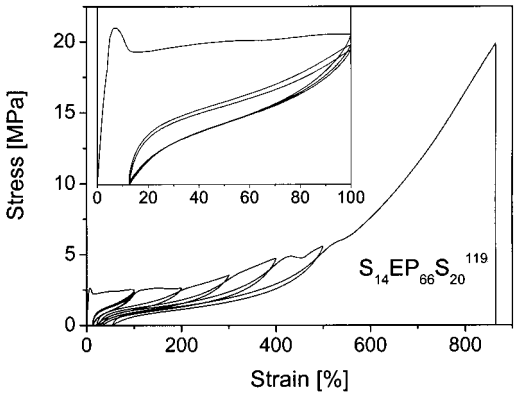

Figure 8. Hysteresis measurements on $S_{14}EP_{66}S_{20}^{119}$.

Figure 7 shows that for extensions to 100% the remaining plastic deformation is nearly constant for all three cycles. The PS-*b*-PEP-*b*-PS triblock copolymer shows a different stress−strain behavior (Figure 8). As can be clearly seen from the inset to Figure 8, a yield point is observed at a strain of 7.7% which may result from the breakup of partially interconnected PS domains (see also Figure 4C). At the yield point formation of a neck occurs, which runs through the sample with increasing strain up to an elongation of ca. 150%. At this point the strain is again distributed homogeneously over the whole sample. In addition, the Young's modulus is much larger as compared to the PS-*b*-PEP-*b*-PE triblock copolymers (Table 3). For well-oriented "single-crystal"-type PS-*b*-PB-*b*-PS triblock copolymers with cylindrical (PS) morphology it is known that the mechanical properties strongly depend on the direction of the applied strain with regard to the oriented PS-cylinders.[37] On elongations parallel to the cylinder axis, the stress−strain curves display a yield behavior, whereas on perpendicular elongations no yield point is observed. Samples of PS-*b*-PEP-*b*-P(S/E) triblock copolymers for TEM and SFM investigations were prepared in a way that we look on the sample along the direction of the afterward applied strain in mechanical testing. For both PS-*b*-PEP-*b*-PS (Figure 4C) and PS-*b*-PEP-*b*-PE (Figure 6A,B) the strongly distorted PS-cylinders show no preferential orientation with respect to the direction of strain (perpendicular to the plane of the TEM or SFM image). Therefore, it can be concluded that the different stress−strain behavior results from differences in the morphology and not from different orientations. In the PS-*b*-PEP-*b*-PS triblock copolymer the PS-cylinders might be partially interconnected, resulting in the observed yielding behavior. In contrast, for PS-*b*-PEP-*b*-PE triblock copolymers the PS and PE domains are dispersed within a matrix of PEP, and no yield point is observed. The observed minimum at 450% strain (Figure 8) arises from the strong tendency of $S_{14}EP_{66}S_{20}^{119}$ to sample slippage especially at high strain values. This effect was also observed for the PE containing triblock copolymers. Compared to $S_{13}EP_{57}E_{30}^{112}$ (Figure 7) and $S_{14}EP_{64}E_{22}^{122}$ (results not shown), the stress values for elongations beyond 100% are always lower for $S_{14}EP_{66}S_{20}^{119}$ (Figure 8). This might result from the suppressed loop formation in PS-*b*-PEP-*b*-PE triblock copolymers due to the strong incompatibility of the end blocks. However, one has to take into account that the morphologies of PS-*b*-PEP-*b*-PS and PS-*b*-PEP-*b*-PE triblock copolymers are not identical.

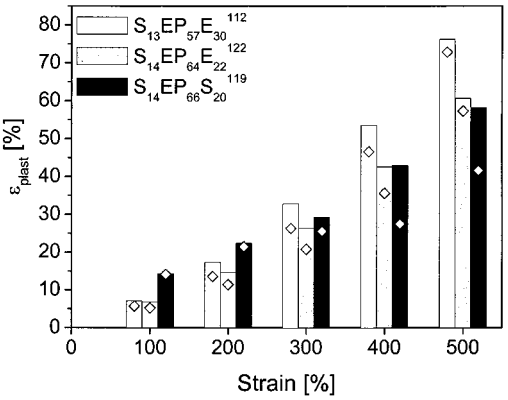

Figure 9. Comparison of plastic deformations (ϵ_{plast}) obtained from hysteresis measurements with (◇) and without (bars) optical extensometers.

Figure 9 shows a comparison of the plastic deformations (ϵ_{plast}) obtained from hysteresis measurements on PS-*b*-PEP-*b*-PS and PS-*b*-PEP-*b*-PE triblock copolymers. For elongations up to 200% both PS-*b*-PEP-*b*-PE triblock copolymers exhibit a smaller plastic deformation (ϵ_{plast}), i.e., better elastic recovery, compared to $S_{14}EP_{66}S_{20}^{119}$ with respect to the measurements conducted without optical extensometers (Figure 9, Table 3). The comparatively high plastic deformation of $S_{14}EP_{66}S_{20}^{119}$ for small strains may also be attributed to the observed necking, which goes along with successive breakup of interconnected PS-cylinders and is expected to continue with increasing strain (postneck or drawing regime), resulting in an accumulation of plastic deformation. Especially the triblock copolymer with a lower PE weight fraction ($S_{14}EP_{64}E_{22}^{122}$) shows better elastic properties, i.e., lower ϵ_{plast}, which is likely to result from a better resistance of the PE crystallites against disruption. Up to 300% strain, the plastic deformation is lower compared to $S_{14}EP_{66}S_{20}^{119}$ and nearly equal for higher strains. A comparison of the plastic deformations of $S_{14}I_{65}S_{21}^{117}$ with $S_{14}EP_{66}S_{20}^{119}$ shows that the non-hydrogenated triblock copolymer exhibits slightly better elastic recovery (Table 3). Annealing of $S_{13}EP_{57}E_{30}^{112}$ at 83 °C for 12 h results in a slight improvement of the elastic recovery, especially at high elongations as depicted in Figure 10. This effect can be attributed to a more uniform crystallite size distribution for the PE block in the annealed sample resulting from the transformation of small (less stable) crystallites into bigger (more stable) ones. This was also detected by DSC, revealing an increased melting temperature of PE and a more narrow melting endotherm in the annealed sample (result not shown).

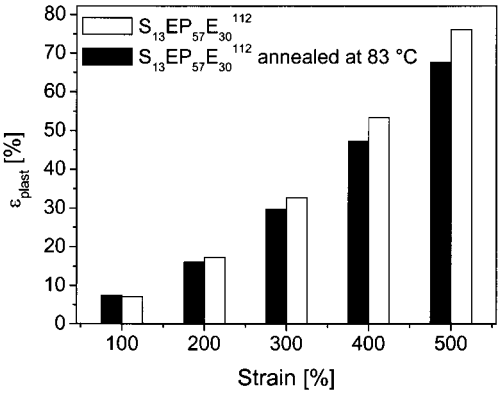

Figure 10. Comparison of plastic deformations (ϵ_{plast}) of $S_{13}EP_{57}E_{30}^{112}$ before and after annealing at 83 °C for 12 h.

One has to take into account that the PS-*b*-PEP-*b*-PS and PS-*b*-PEP-*b*-PE triblock copolymers show slippage especially at high elongations which strongly affects the determined plastic deformations. Therefore, we also conducted hysteresis measurements with optical extensometers which are insensitive to sample slippage. The obtained plastic deformations are depicted as diamonds in Figure 9. For strains up to 300% the use of optical extensometers confirms the behavior described above. In contrast, for higher elongations the recovery of $S_{14}EP_{66}S_{20}^{119}$ gets significantly better compared to the PE-containing triblock copolymers, reflecting the strong effect of slippage observed for $S_{14}EP_{66}S_{20}^{119}$ on the measurements without optical extensometers.

In conclusion, for strains up to 300% PS-*b*-PEP-*b*-PE triblock copolymers exhibit a slightly improved elastic recovery compared to the PS-*b*-PEP-*b*-PS triblock copolymer. However, for higher strains the PE crystallites in PS-*b*-PEP-*b*-PE triblock copolymers apparently suffer greater distortions than the amorphous PS domains in the PS-*b*-PEP-*b*-PS triblock copolymer leading to higher plastic deformations. The improved elastic recovery at low strains for the PE containing triblock copolymers might be attributed to the suppressed loop formation in this system due to the strong incompatible end blocks. Another possibility for the observed behavior might arise from the different morphologies of PS-*b*-PEP-*b*-PS and PS-*b*-PEP-*b*-PE triblock copolymers. In addition, the observed yielding and necking for $S_{14}EP_{66}S_{20}^{119}$ and $S_{14}I_{65}S_{21}^{117}$ triblock copolymers, which might be related to the breakup of interconnected PS-cylinders, also results in an increased plastic deformation.

In general, for PS-*b*-PEP-*b*-PE triblock copolymers the elastic recovery is better for systems with a lower PE weight fraction. This result is in agreement with the results obtained by Morton et al. for PE-*b*-PI-*b*-PE and PE-*b*-PEB-*b*-PE triblock copolymers.[29−31] The investigated triblock copolymers with approximately 30 wt % PE exhibit relatively good elastic recovery, whereas the systems with higher PE contents show unusually high unrecovered deformations, i.e., cold drawing. For high strains they have also detected a much higher plastic set for the PE containing triblock copolymers compared to PS-*b*-PB-*b*-PS triblock copolymers, which was attributed to a smaller resistance of the PE crystallites against distortion compared to amorphous PS domains, especially at high elongations.

Conclusions

We have compared the morphologies and mechanical properties of PS-*b*-PEP-*b*-PE triblock copolymers with a PS-*b*-PI-*b*-PS and the corresponding hydrogenated PS-*b*-PEP-*b*-PS triblock copolymer. SFM investigations on PS-*b*-PEP-*b*-PE triblock copolymers in combination with selective swelling of the PS domains by exposure to toluene vapor enables us to simultaneously detect the PS and PE domains which is not possible by using conventional TEM techniques. Because of the imcompatibility of the end blocks, the formation of loops is suppressed, resulting in a morphology consisting of dispersed PS cylinders and PE crystallites within a matrix of the PEP block. Morphological investigations on compression-molded samples exhibit a distorted cylindrical structure of the PS block for PS-*b*-PI-*b*-PS and PS-*b*-PEP-*b*-PS, making the formation of loops and interconnected PS cylinders possible.

Comparison of plastic deformations obtained from hysteresis measurements on PS-*b*-PEP-*b*-PE and PS-*b*-PEP-*b*-PS triblock copolymers reveals better elastic properties, i.e., smaller plastic deformations, of the PE containing triblock copolymers at small strains. Different reasons may be responsible for that: the restricted loop formation in PS-*b*-PEP-*b*-PE triblock copolymers, the different morphologies of the compared systems, or a combination of both effects. In contrast to the behavior at small strains, for high strain values the PS-*b*-PEP-*b*-PS triblock copolymer exhibits a significantly better elastic recovery. This might be attributed to a weaker resistance of crystalline PE domains against disruption compared to amorphous PS domains. In general, the elastic recovery of PS-*b*-PEP-*b*-PE triblock copolymers improves with decreasing content of crystalline PE.

Acknowledgment. We thank K. Matussek, R. Giesa, and J. van Elburg for assistance with mechanical testing, A. J. Müller (Universidad Simón Bolívar, Caracas) for helpful discussions concerning the DSC measurements, C. Drummer for SEM, and A. Göpfert for TEM investigations. Financial support was given by DSM Research, Geleen, and the German Israeli Foundation for Scientific Research and Development (GIF). This work was partially supported by the Deutsche Forschungsgemeinschaft (SFB 481) and by the Bayreuther Institut für Makromolekülforschung (BIMF).

References and Notes

(1) Morton, M. *Encyclopedia of Polymer Science and Technology*; John Wiley & Sons: New York, 1971; Vol. 15, p 508.
(2) Morton, M. *Anionic Polymerization: Principles and Practice*; Academic Press: New York, 1983.
(3) Holden, G.; Legge, N. R. Styrenic Thermoplastic Elastomers. In *Thermoplastic Elastomers: A Comprehensive Review*, 2nd ed.; Holden, G., Legge, N. R., Quirk, R. P., Schroeder, H. E., Ed.; Hanser: Munich, 1996; p 47.
(4) Mogi, Y.; Nomura, M.; Kotsuji, H.; Ohnishi, K.; Matsushita, Y.; Noda, I. *Macromolecules* **1994**, *27*, 6755.
(5) Riess, G.; Hurtrez, G.; Bahadur, P. *Encycl. Polym. Sci. Eng.* **1985**, *2*, 324.
(6) Bates, F. S.; Fredrickson, G. H. *Phys. Today* **1999**, *52*, 32.
(7) Abetz, V. In *Supramolecular Polymers*; Ciferri, A., Ed.; Marcel Dekker: New York, 2000; Chapter 6, p 215.
(8) Kane, L.; Spontak, R. J. *Macromolecules* **1994**, *27*, 663.
(9) Stadler, R.; Auschra, C.; Beckmann, J.; Krappe, U.; Voigt-Martin, I.; Leibler, L. *Macromolecules* **1995**, *28*, 3080.
(10) Gido, S. P.; Schwark, D. W.; Thomas, E. L.; do Carmo Goncalves, M. *Macromolecules* **1993**, *26*, 2636.
(11) Breiner, U.; Krappe, U.; Abetz, V.; Stadler, R. *Macromol. Chem. Phys.* **1997**, *198*, 1051.
(12) Breiner, U.; Krappe, U.; Jakob, T.; Abetz, V.; Stadler, R. *Polym. Bull.* **1998**, *40*, 219.
(13) Shefelbine, T. A.; Vigild, M. E.; Matsen, M. W.; Hajduk, D. A.; Hillmyer, M. A.; Cussler, E. L.; Bates, F. S. *J. Am. Chem. Soc.* **1999**, *121*, 8457.

(14) Abetz, V.; Goldacker, T. *Macromol. Rapid Commun.* **2000**, *21*, 16.
(15) Hückstädt, H.; Göpfert, A.; Abetz, V. *Polymer* **2000**, *41*, 9089.
(16) Breiner, U.; Krappe, U.; Stadler, R. *Macromol. Rapid Commun.* **1996**, *17*, 567.
(17) Breiner, U.; Krappe, U.; Thomas, E. L.; Stadler, R. *Macromolecules* **1998**, *31*, 135.
(18) Ott, H.; Abetz, V.; Altstädt, V. *Macromolecules* **2001**, *34*, 2121.
(19) Abetz, V.; Stadler, R.; Leibler, L. *Polym. Bull.* **1996**, *37*, 135.
(20) Brinkmann, S.; Stadler, R.; Thomas, E. L. *Macromolecules* **1998**, *31*, 6566.
(21) Brinkmann-Rengel, S.; Abetz, V.; Stadler, R.; Thomas, E. L. *Kautschuk Gummi Kunststoffe* **1999**, *52*, 806.
(22) Kofinas, P.; Cohen, R. E. *Macromolecules* **1994**, *27*, 3002.
(23) Rangarajan, P.; Register, R. A.; Fetters, L. J. *Macromolecules* **1993**, *26*, 4640.
(24) Rangarajan, P.; Register, R. A.; Adamson, D. H.; Fetters, L. J.; Bras, W.; Naylor, S.; Ryan, A. J. *Macromolecules* **1995**, *28*, 1422.
(25) Bates, F. S.; Schultz, M. F.; Rosedale, J. H. *Macromolecules* **1992**, *25*, 5547.
(26) Falk, J. C. *Macromolecules* **1971**, *4*, 152.
(27) Falk, J. C.; Schlott, R. J. *Angew. Makromol. Chem.* **1972**, *21*, 17.
(28) Mohajer, Y.; Wilkes, G. L.; Wang, I. C.; McGrath, J. E. *Polymer* **1982**, *23*, 1523.
(29) Morton, M.; Lee, N.-C.; Terrill, E. R. *Polym. Prepr.* **1981**, *22*, 136.
(30) Morton, M.; Lee, N.-C.; Terrill, E. R. *ACS Symp. Ser.* **1982**, *193*, 101.
(31) Morton, M. *Rubber Chem. Technol.* **1983**, *56*, 1096.
(32) Morton, M.; Quirk, R. P. Anionic Triblock Copolymers. In *Thermoplastic Elastomers: A Comprehensive Review*, 2nd ed.; Holden, G., Legge, N. R., Quirk, R. P., Schroeder, H. E., Eds.; Hanser: Munich, 1996; p 71.
(33) Séguéla, R.; Prud'homme, J. *Polymer* **1989**, *30*, 1446.
(34) Brandrup, J.; Immergut, E. H. *Polymer Handbook*, 3rd ed.; Wiley: New York, 1989.
(35) Park, C.; De Rosa, C.; Fetters, L. J.; Thomas, E. L. *Macromolecules* **2000**, *33*, 7931.
(36) Elbs, H.; Fukunaga, K.; Stadler, R.; Sauer, G.; Magerle, R.; Krausch, G. *Macromolecules* **1999**, *32*, 1204.
(37) Odell, J. A.; Keller, A. *Polym. Eng. Sci.* **1977**, *17*, 544.

MA010875D